Computación y Sistemas
ISSN: 1405-5546
computacion-y-sistemas@cic.ipn.mx
Instituto Politécnico Nacional
México

Mendiola-Santibañez, Jorge Domingo; Arias-Estrada, Miguel Octavio; Santillán-Méndez, Israel Marcos; Rodríguez-Reséndiz, Juvenal; Gallegos-Duarte, Martín; Gómez-Meléndez, Domingo José; Terol-Villalobos, Iván Ramón

Morphological Filtering Algorithm for Restoring Images Contaminated by Impulse Noise
Computación y Sistemas, vol. 19, núm. 2, 2015, pp. 243-254
Instituto Politécnico Nacional
Distrito Federal, México

Available in: http://www.redalyc.org/articulo.oa?id=61539886004

ISSN 2007-9737

Morphological Filtering Algorithm for Restoring Images Contaminated by Impulse Noise

Jorge Domingo Mendiola-Santibañez[1,3], Miguel Octavio Arias-Estrada[2], Israel Marcos Santillán-Méndez[3], Juvenal Rodríguez-Reséndiz[3], Martín Gallegos-Duarte[4], Domingo José Gómez-Meléndez[5], Iván Ramón Terol-Villalobos[1]

[1] Centro de Investigación y Desarrollo Tecnológico en Electroquímica, Querétaro, Mexico

[2] Instituto Nacional de Astrofísica, Óptica y Electrónica, Coordinación de Ciencias Computacionales, Puebla, Mexico

[3] Universidad Autónoma de Querétaro, Facultad de Ingeniería, Querétaro, Mexico

[4] Universidad Autónoma de Querétaro, Doctorado de la Facultad de Medicina, Querétaro, México

[5] Universidad Politécnica de Querétaro, Querétaro, Mexico

mendijor@uaq.mx, ariasmo@inaoep.mx, santilis@gmail.com,juvenal@ieee.org, martin_oso@hotmail.com, domag5@hotmail.com, iterol@cideteq.mx

Abstract. In this paper a methodology to restore gray scale images with pixels polluted by random impulsive noise is presented. Noise is discovered using a criterion based on the white top-hat by reconstruction. Pixels detected as corrupted are restored using an iterative morphological algorithm built with extensive and antiextensive morphological transformations. The proposal is compared with the rank ordered mean filter (ROM) and other morphological transformations reported in the current literature.

Keywords. Noise detection, morphological pixel restoration, transformations by reconstruction.

1 Introduction

The goal of impulse noise removal in images is to suppress the noise while preserving the integrity of edge and detail information. To reach this goal, nonlinear techniques have been found to provide more satisfactory results in comparison with linear methods. For instance, median and, in general, order statistic filters have demonstrated good performance in the removal of impulse noise [2, 4, 5, 7, 12].

However, since these approaches are typically implemented uniformly across an image, they tend to modify pixels that are undisturbed by noise. Consequently, an effective removal of impulses is often performed at the expense of blurred and distorted features. In [11], the author introduces a method where outliers are replaced by estimating a regularization term. In particular, smooth and convex edge-preserving potential functions are used.

The idea given in [11] is utilized in [3] to remove noisy components. The disadvantage of the proposal given in [3] is the way of suppressing noise, since it is not clear how the authors detect the

best threshold parameter related to noise distribution. On the other hand, a filter used to remove impulse noise with percentages as much as 40% is reported in [1]. This filter is called the rank-ordered-mean filter (ROM) and it is built similar to the mean operator but without including the center pixel, i.e., the noisy pixel is eliminated during the processing.

Within Mathematical Morphology (MM), some special operators used for suppressing random impulsive noise are the rank-max connected opening [10], morphological amoebas [8], the opening and closing by reconstruction [16], and the area opening [17], among others. All of them have the characteristic of being adaptive. Nevertheless, these transformations are applied once on the whole image without considering a restoration process.

Due to this fact, a new approach to deal with the elimination of impulse noise from the MM point of view is introduced in this paper. The proposal includes the following steps: i) noise detection; ii) filtering of corrupted regions, and iii) restoration by means of extensive and antiextensive connected transformations. On the other hand, the opening and closing by reconstruction fulfill transformations to be connected [13], i.e., they avoid the creation of new information during the processing.

However, these operators cannot process adequately long and narrow regions, this problem is due to the fact that the structuring element does not fit these structures. Nevertheless, all regions where the structuring element fits will be preserved. Due to this fact, in the present paper, the opening and closing by reconstruction will be used to restore the image, and the median operator will filter the noisy components. At this point, a problem with our proposal is that it cannot adequately preserve the details of the image.

The paper is organized as follows: Sections 2.1 and 2.2 define the operators utilized throughout the text. The method to detect noise is given in Section 2.3. The iterative process to make the restoration is outlined in Section 2.4. In Section 2.5, the results obtained in this study are compared against the morphological rank filter, morphological amoebas, and the ROM filter on images contaminated with different noise percentages. Discussion is presented in Section 3 and conclusions are given in Section 4.

2 Morphological Methodology to Suppress Impulse Noise

2.1 Definitions of Some Morphological Transformations

The basic morphological filters are the morphological opening $\gamma_{\mu B}(f)$ and closing $\varphi_{\mu B}(f)$ [6]. In this paper, a square structuring element is employed, where B represents the basic structuring element of size 3×3 pixels, which contains its origin. While $\breve{B}$ is the transposed set with respect to its origin, $\breve{\mathrm{B}}=\{-\mathrm{x} : \mathrm{x} \in \mathrm{B}\}$, $\mu \in Z$ is a size parameter, and Z represents the integers set. The morphological opening $\gamma_{\mu B}(f)$ is expressed as $\gamma_{\mu B}(f)(x) = \delta_{\mu B}(\varepsilon_{\mu \breve{B}}(f))(x)$. By duality, the morphological closing $\varphi_{\mu B}(f)$ is defined as $\varphi_{\mu B}(f)(x) = [\gamma_{\mu B}(f^c)]^c$, where $f^c(x) = 255 - f(x)$, $\delta_{\mu B}$, and $\varepsilon_{\mu B}(f)$ represent the morphological dilation and erosion $\varepsilon_{\mu B}(f)(x) = \bigwedge\{f(y) : y \in \mu\breve{B}_x\}$, and $\bigwedge$ denotes the inf operator. By duality, the morphological dilation is written as $\delta_{\mu B}(f)(x) = [\varepsilon_{\mu B}(f^c)(x)]^c$.

2.2 Opening by Reconstruction

Transformations by reconstruction are built with geodesic transformations [11]. The geodesic dilation $\delta_f^1(g)(x)$ is given by $\delta_f^1(g)(x)$=$f(x) \wedge \delta(g)(x)$ with $g(x) \leq f(x)$. When the marker $g(x)$ is equal to the erosion of the original function $\varepsilon_{\mu B}(f)(x)$, and the geodesic dilation is iterated until the idempotence is reached, the opening by reconstruction $\tilde{\gamma}_{\mu B}(f)$ is obtained, where $\tilde{\gamma}_{\mu B}(f)(x) = lim_{n\to\infty}\, \delta_f^n(\varepsilon_{\mu B}(f))(x)$. By duality, the closing by reconstruction $\tilde{\varphi}_{\mu B}(f)$ is represented as $\tilde{\varphi}_{\mu B}(f)(x) = (\tilde{\gamma}_{\mu B}(f^c)(x))^c$. The opening by reconstruction accomplishes to be an antiextensive transformation, $\tilde{\gamma}_{\mu B}(f) \leq f$, while the closing by reconstruction fulfills the property to be extensive, i.e., $\tilde{\varphi}_{\mu B}(f) \geq f$. Fig. 1 illustrates these properties. In Fig. 1(d) notice that the original image f is comprised between the closing and opening by reconstruction. This special feature will be used in Section 2.4 to introduce a morphological restoration method. On the other hand, reconstruction transformations do not introduce new information; Figures 1(b) and 1(c) exemplify this

fact, note that the maxima or minima have been flattened, however, the remaining components stay unchanged during the processing, thus ensuring the preservation of the edges.

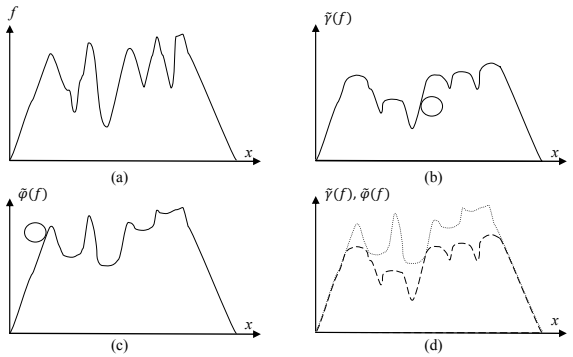

Fig. 1. Extensive and antiextensive transformations. (a) Original image f; (b) opening by reconstruction using a circular flat structuring element B, $\tilde{\gamma}_B(f) \leq f$; (c) closing by reconstruction using a circular flat structuring element B, $\tilde{\varphi}_B(f) \geq f$; (d) opening and closing by reconstruction, $\tilde{\varphi}_\mu(f) \geq f \geq \tilde{\gamma}_\mu(f)$

2.3 Noise Detection

The white top-hat by reconstruction is defined as [15]: $\tilde{T}W_\mu(f) = f - \tilde{\gamma}_\mu(f)$. Hence, a criterion to detect impulsive noise is defined by the formula that follows [9]. A pixel $f(x)$ is corrupted if

$$\tilde{T}W_\mu(f)(x) \geq \overline{\tilde{T}W}_\mu(f)(x), \tag{1}$$

with $\overline{\tilde{T}W}_\mu(f)$ being the mean white top-hat by reconstruction. This criterion allows detecting noise in white components, for this, the complement image also should be processed to filter the dark components using the same criterion. The candidate noise set ρ is defined as

$$\rho = \{ z \in D_f : \tilde{T}W_\mu(f)(z) \geq \overline{\tilde{T}W}_\mu(f)(z)$$

and

$$\tilde{T}W_\mu(f^c)(z) \geq \overline{\tilde{T}W}_\mu(f^c)(z)\},$$

whereas $\rho^c = D_f \setminus \rho$ represents the set of all uncorrupted pixels.

2.4 Morphological Image Restoration

To restore gray level intensities, firstly, noise candidates are identified by using the procedure outlined in Section 2.3, and all pixels detected as uncorrupted will keep their values during the processing. Posteriorly, the restoration process based on extensive and antiextensive filters by reconstruction is applied to find adequate values for those pixels classified as corrupted. Two images, $CP: Z^2 \rightarrow Z$ and *UCP:*$Z^2 \rightarrow Z$, are defined, CP represents the Corrupted Pixels Image, this image is initialized with zeros and filled with the corrupted pixels, $\forall\ z \in \rho$. The Uncorrupted Pixels Image *UCP* is initialized with zeros and posteriorly filled by the uncorrupted pixels, $\forall\ \hat{z} \in \rho^c$. The input image f can be represented as

$$f = UCP + CP.$$

The original image f is filtered using the median filter $M_{\mu=1}(f)$, $\mu = 1$. The operator $M_{\mu=1}$ smooths several regions, in consequence flat zones will be produced. Then, the corrupted pixels are replaced by the filtered gray levels obtained from the transformation $M_{\mu=1}(f)$, while the uncorrupted pixels are maintained unchanged, $\forall\ \hat{z} \in \rho^c$. The symbol $\mathcal{N}$ indicates that the image $M^{\mathcal{N}}_{\mu=1}(f)$ contains zeros $\forall\ \hat{z} \in \rho^c$ and that the median values are maintained in the positions $z \in \rho$. The new output image is expressed as

$$\eta = UCP + M^{\mathcal{N}}_{\mu=1}(f). \tag{2}$$

As a first approximation, noise elimination is done using Eq. 2. An example of applying Eq. 2 is presented in Fig. 3, where several white components on the coat appear due to the median filter performance, i.e., this transformation tends to create new information. In order to restore all pixels located in the position $y \in \rho$, the following correction is made in Eq. 2:

$$\eta^* = \mathrm{UCP} + \chi^{\mathcal{N}}, \tag{3}$$

where $\chi^{\mathcal{N}}$ is defined as

$$\chi^{\mathcal{N}} = (\widetilde{\gamma}_{\mu=1}(\eta))^{\mathcal{N}} + \left(\frac{\widetilde{\varphi}_{\mu=1}(\eta) - \widetilde{\gamma}_{\mu=1}(\eta)}{2}\right)^{\mathcal{N}}. \tag{4}$$

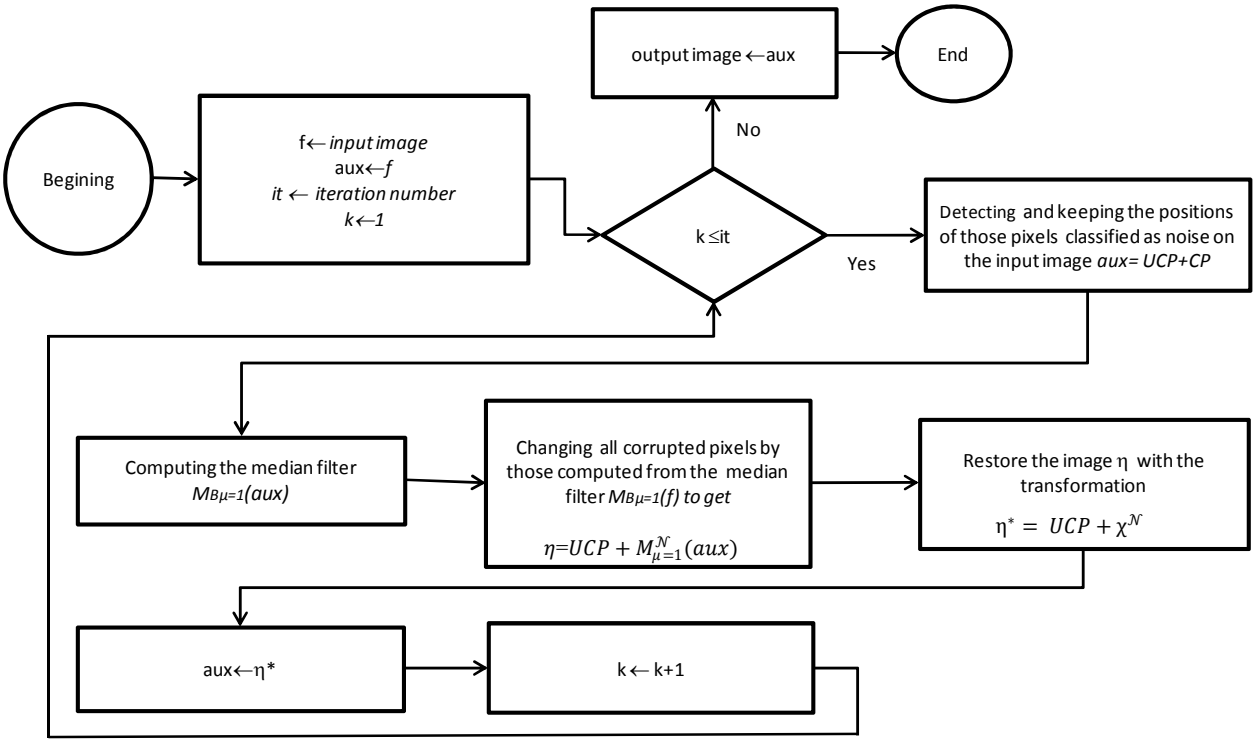

Fig. 2. Flow diagram to implement Equations 2 and 3 iteratively

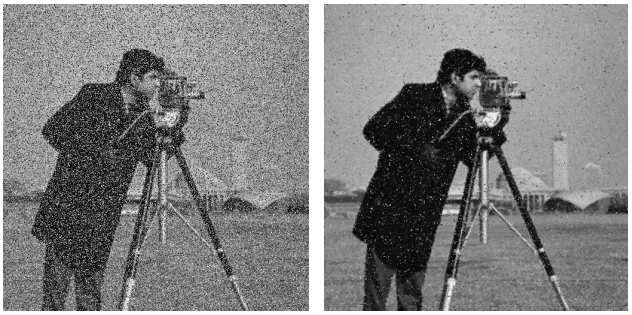

(a) (b)

Fig. 3. Noise elimination using Eq. 2. (a) Input image with 40% random impulse noise; (b) image where noise has been eliminated

The term $\chi^{\mathcal{N}}$ modifies the gray level of those pixels whose positions were classified as corrupted. Notice that

$$\widetilde{\gamma}_{\mu=1}(\eta) \leq \chi^{\mathcal{N}}_{\mathrm{k}=1} \leq \widetilde{\varphi}_{\mu=1}(\eta)\,.$$

Equations 2 and 3 can be iterated k times to obtain better results. A flow diagram representing this procedure is presented in Fig. 2, while Fig. 4 shows an example considering 10 iterations. The input image is given in Fig. 3(a).

Notice in Fig. 4 that several regions located in Fig. 3(b) have been restored and the contours around the coat are modified. The creation of artifacts is due to the median filter. On the other hand, the computed term $\chi^{\mathcal{N}}$ for a certain k value allows improving the $PSNR$ index as k is increased. To corroborate this situation, the PSNR index is estimated at each iteration giving as result the data set presented in Table 1 and its respective graph in Fig. 5.

The graph in Fig. 5 shows that the quality of the image is improved as k is increased. It is important to mention that η^* reaches the $n-idempotence$ for the value $k=n$, i.e., $\eta^*_n\eta^*_{n+1}$=η^*_n.

It can be seen in Table 1 that this property is fulfilled for $k=8$, however, the $n-idempotence$ de-

Fig. 4. Output image after iterating 10 times the algorithm implemented according to the flow diagram presented in Fig. 2

pends of the information of each processed image. A practical way to identify it consists in evaluating the sum of all gray levels of the processed image: when the sum does not change for the following iteration, the $n - idempotence$ is reached.

Table 1. PSNR values considering 10 iterations

k	PSNR
0	22.507
1	23.847
2	24.295
3	24.433
4	24.477
5	24.492
6	24.500
7	24.503
8	24.503
9	24.503
10	24.503

2.5 Experimental Results

In this section, the performance of Equations 3 and 4 applied iteratively is compared against other specialized transformations reported in the literature. In Fig. 6 an example is presented. The input image is contaminated with 60% random impulsive noise, see Fig. 6(a). The output image obtained from the connected rank-max opening is given in Fig. 6(b) considering $\mu = 3$ and the connected filter associated to the position $k = 20$. In Fig. 6(c) morphological amoebas are computed using $\mu = 5$

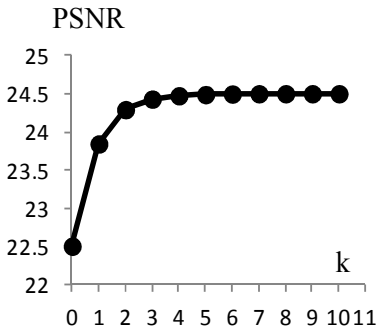

Fig. 5. Graph corresponding to the values given in Table 1

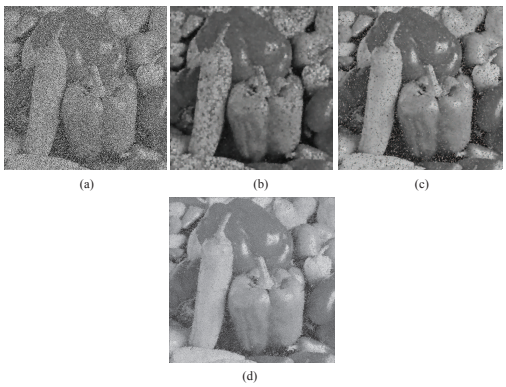

Fig. 6. Comparison with other methodologies. (a) Image contaminated with 60% random impulse noise; (b) rank max connected opening; (c) morphological amoebas, (d) proposal given in this paper according to the flow diagram given in Fig. 2 considering 10 iterations

and $\lambda = 0.02$. The image in Fig. 6(d) corresponds to the algorithm implemented according to the flow diagram given in Fig. 2 applying 10 iterations. Measurements corresponding to the PSNR and SSIM [18] indices for images in Fig. 6 are displayed in Table 2. Better values for the SSIM index are those closest to 1. It can be observed in Table 2 that the adaptive transformations, rank max, and morphological amoebas present good performance, however, the problem with these operators is that they are applied once on the whole image causing a modification of corrupted and uncorrupted pixels at the same time. On the contrary, our proposal modifies and restores only the detected noisy pixels in each iteration. On the other hand, a problem with

Table 2. PSNR and SSIM indices associated to the images in Fig.6

Image	PSNR	SSIM
Fig. 6(b)	18.5756	0.5512
Fig. 6(c)	24.4405	0.3883
Fig. 6(d)	25.0975	0.6632

Table 3. PSNR and entropy (H) values for the images in Fig 8 and for the original images in Fig. 7

Figure	PSNR	H
7(a)	∞	2.9920
8(a1)	24.5736	3.0408
8(a2)	25.6289	3.2838
8(a3)	23.0061	5.4107
8(a4)	24.5752	3.5385
7(b)	∞	1.7185
8(b1)	28.6544	1.6200
8(b2)	31.4726	1.7122
8(b3)	28.8863	2.7666
8(b4)	30.4651	1.6254
7(c)	∞	3.1969
8(c1)	26.7877	3.2583
8(c2)	28.4348	3.4134
8(c3)	25.6786	5.3318
8(c4)	27.4307	3.5626
7(d)	∞	2.5948
8(d1)	28.1209	2.6216
8(d2)	30.9022	2.7682
8(d3)	27.7226	4.5647
8(d4)	29.8351	2.8357
7(e)	∞	3.6756
8(e1)	24.0993	3.8113
8(e2)	25.3106	4.0435
8(e3)	23.0669	6.4146
8(e4)	24.1939	4.4497

the SSIM index is that sometimes this measure does not coincide with the visual perception of the processed image; so in the next example this index will not be computed. Another example is implemented considering 10% and 40% random impulsive noise. The set of original images to carry out this experiment was taken from the USC-SIPI Image Database (http://sipi.usc.edu/database/), see Fig 7(a)-(e).

These images were contaminated with impulse noise using Matlab, and they are shown in Figures 7(f)-7(j) and 7(k)-(o). The filters to be compared with our proposal are the median and the ROM filters [1]. The experiments consist in a) applying the median filter, our proposal, and the ROM filter

Table 4. PSNR and entropy (H) values for the images in Fig 9 and for the original images in Fig. 7

Figure	PSNR	H
7(a)	∞	2.9920
9(a1)	20.0937	4.1728
9(a2)	22.1535	3.6385
9(a3)	21.0684	6.2651
9(a4)	22.4495	4.6001
7(b)	∞	1.7185
9(b1)	23.2744	1.6200
9(b2)	28.5185	1.7625
9(b3)	28.0764	3.6703
9(b4)	28.6784	2.3248
7(c)	∞	3.1969
9(c1)	22.3572	4.0746
9(c2)	24.9504	3.6871
9(c3)	23.7828	6.2927
9(c4)	25.1127	4.5027
7(d)	∞	2.5948
9(d1)	24.5265	3.3448
9(d2)	27.6297	2.9657
9(d3)	26.2917	5.5456
9(d4)	27.9095	3.7170
7(e)	∞	3.6756
9(e1)	20.4768	4.7309
9(e2)	22.3540	4.4465
9(e3)	21.3413	7.2344
9(e4)	22.4938	5.5581

3 times on the whole image, and b) the restoration of those pixels classified as noise considering the information provided by the ROM filter. Figures 8 and 9 display the output images. Tables 3 and 4 present the PSNR and entropy [14] (denoted as H) indices. Entropy is used to compare the similarity between two pixels. The following observations correspond to the computed indices:

— According to the PSNR values shown in Table 3, our method outperforms the median and ROM transformations for the set of images contaminated with 10% noise. Table 4, which corresponds to the set of images corrupted with 40% noise, indicates that the sequential application of the ROM filter presents a better behavior compared with the other transformation.

— The H index in the literature is used as a measure of the details and the similarity between two pixels. However, H is expressed in terms of probability and the logarithm of

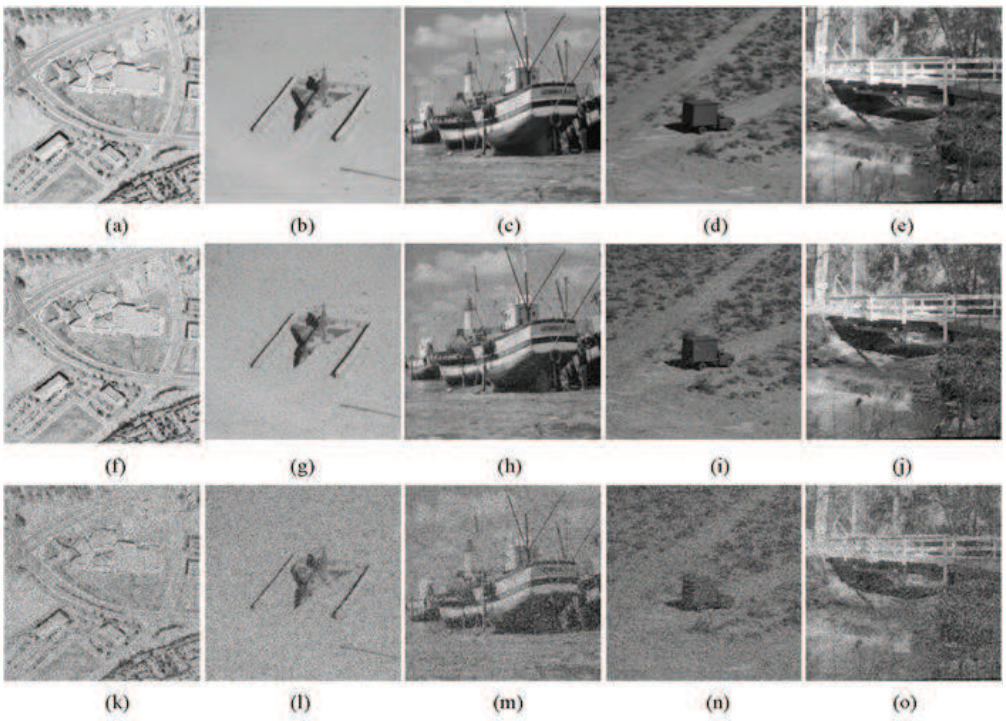

Fig. 7. Set of images used to illustrate the performance of the proposal given in this paper. (a)-(e) Original images obtained from the USC-SIPI Image Database; (f)-(j) images contaminated with 10% random impulse noise; (k)-(o) images contaminated with 40% random impulse noise

the same probability. Then, lower values of H in the experiment presented here indicate that the processed image has been smoothed considerably with respect to the other methods. In Table 3, the higher values of entropy correspond to the ROM filter when it is applied on the whole image 3 times, followed by the iterative ROM filter applied 3 times uniquely on noisy pixels, then our method, and, lastly, the median filter. In Table 4, the index H has a similar behavior to that in Table 3. Since our method presents a low H compared to the ROM filter when it is applied 3 times uniquely on noise pixels, the obtained output image is more smoothed. For this reason the PSNR values are better for the ROM filter in Table 4.

It can be observed in Table 4 that the ROM filter iterated sequentially on noisy pixels has a better performance when the noise percentage is increased, and when the noise percentage decreases, see Table 3, the proposal given in this paper shows a better performance.

It is important to mention here that the flow diagram presented in Fig. 2 is implemented in Matlab which includes fast algorithms for computing the opening and closing by reconstruction. A deep study on implementation of geodesic transformations can be found in [16], where the order associated with these operators is not reported. The difficulty in obtaining the order is that it depends on the processed image: for example, the opening by reconstruction consumes more time as the number of regional maxima is increased. Therefore, in this paper the execution time is obtained for the algorithm represented by the flow diagram considering 6 iterations. The algorithm is implemented in Matlab R2010a on a 2.5 GHz Intel Core i5 processor with 2 GB RAM memory. The measures are presented in Table 5 together with the time

ISSN 2007-9737

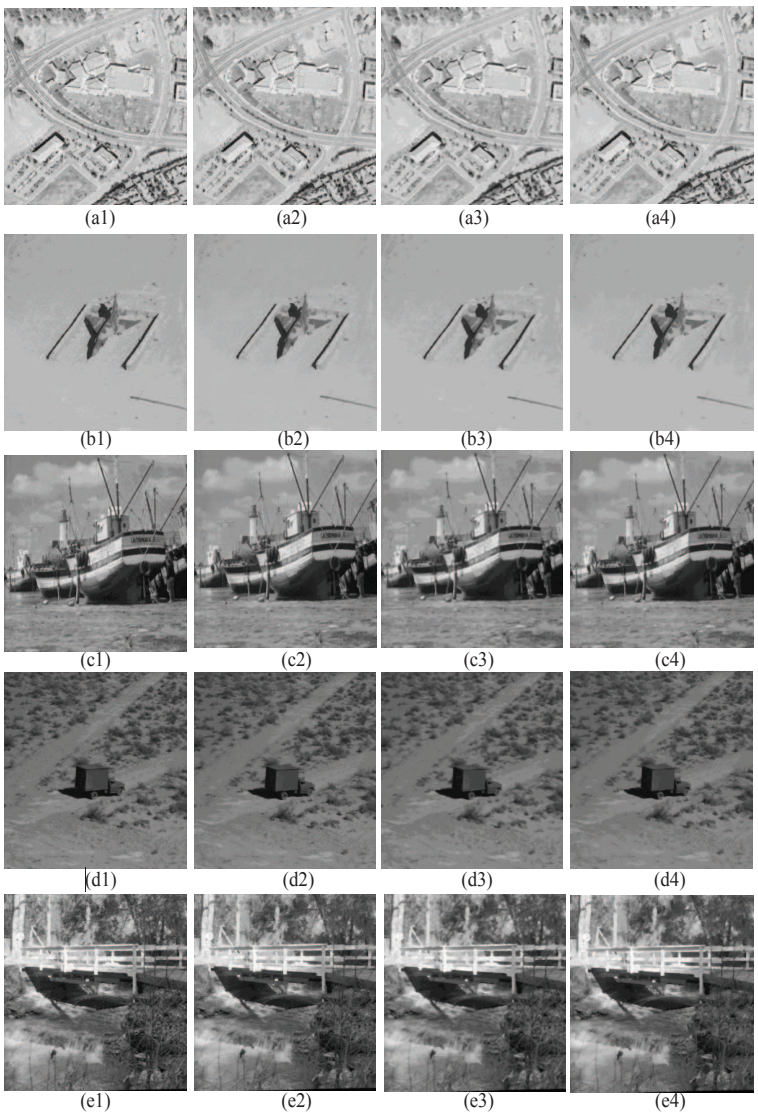

Fig. 8. Filtered images considering 10% of contamination. The filter associated to the output images in each row is (a1),(b1),(c1),(d1),(e1) median filter with a window of 3×3 elements applied 3 times; (a2),(b2),(c2),(d2),(e2) the proposal given in this paper with 3 iterations; (a3),(b3),(c3),(d3),(e3) ROM filter with a window of 3×3 elements applied 3 times; (a4),(b4),(c4),(d4),(e4) only noisy pixels are restored using the ROM filter during 3 iterations

associated to the ROM filter considering the same number of iterations. The experiment considers the images in Figures 8(k) and 8(l). The graph of the values reported in this table can be seen in Fig. 10.

It can be seen in Table 5 that for all k values the ROM filter applied 3 times on the whole image is faster than our proposal. On the other hand, for our algorithm, if the parameter k is increased, the n-idempotence will be reached at a certain moment and there will be no changes in time.

Additionally, our method spends more time during the iteration process because it is necessary to identify the positions of the noisy pixels. In each iteration, the number of corrupted pixels decreases,

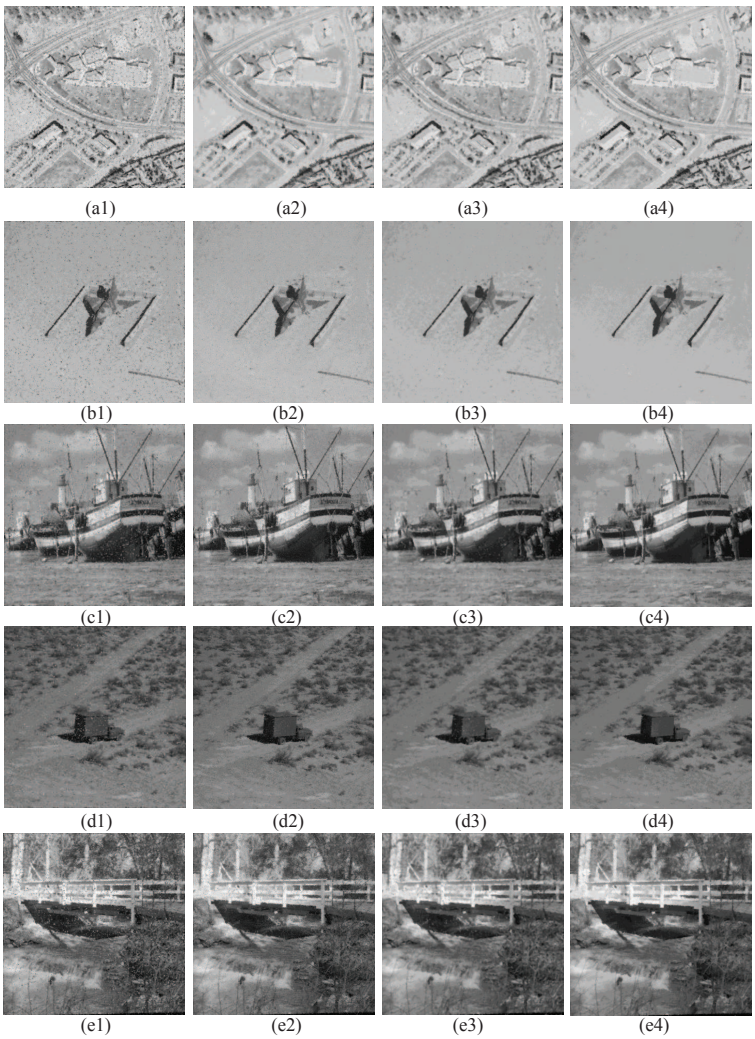

Fig. 9. Filtered images considering 40% of contamination. The filter associated to the output images en each row is (a1),(b1),(c1),(d1),(e1) median filter with a window of 3×3 elements applied 3 times; (a2),(b2),(c2),(d2),(e2) the proposal given in this paper considering 3 iterations; (a3),(b3),(c3),(d3),(e3) ROM filter with a window of 3×3 elements applied 3 times; (a4),(b4),(c4),(d4),(e4) noisy pixels are restored using the ROM filter during 3 iterations

and the algorithm runs almost at the same speed as k is increased. This behavior can be observed for $k > 3$ in the graphs displayed in Fig. 10. A similar behavior is presented by the ROM filter when it is iterated sequentially to restore noisy pixels only.

3 Discussion

Now we will discuss the advantages and disadvantages of our proposal. The advantages are:

1. According to the computed PSNR indices, our proposal presents a better development than the median and ROM filters for images contaminated with 10% noise. This occurs be-

Table 5. Execution time in minutes (min) utilized to process the images 8(k) and 8(l)

Iteration	A	B	C	D	E	F
1	0,52	0,52	0,17	0,19	0,48	0,50
2	0,82	0,84	0,29	0,28	0,88	0,70
3	0,95	0,83	0,41	0,41	1,09	1,00
4	1,00	0,84	0,56	0,53	1,16	1,08
5	1,06	0,87	0,69	0,69	1,31	1,16
6	1,10	0,88	0,84	0,78	1,44	1,36

A: Image in Fig 8(k) using our proposal; B: Image in Fig 8(l) using our proposal; C:Image in Fig 8(k) using ROM filter on the whole image; D:Image in Fig 8(l) using ROM filter on the whole image; E:Image in Fig 8(k) using ROM filter sequentially on noisy pixels; F:Image in Fig 8(l) using ROM filter sequentially on noisy pixels

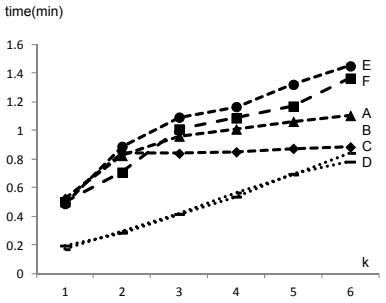

Fig. 10. Graph of the values presented in Table 5

cause the restoration process permits to detect a better pixel value.

2. The flow diagram presented in Fig. 2 can be implemented in Matlab because fast algorithms for the opening and closing by reconstruction transformations are included in this software.

3. Due to elimination of only noise, i.e., when elimination is done considering only those pixels detected as corrupted, the various structures composing the image are better preserved.

4. At each iteration, the pixels detected as noise not only are replaced by some gray level computed from the median filter, but a restoration is made considering Eq. 4.

5. The opening and closing by reconstruction try to avoid the creation of new information.

The disadvantages are as follows:

1. According to the computed PSNR indices in Table 4 (corresponding to images contaminated with 40% noise), the ROM filter presents a better development than our proposal when it is applied iteratively on noisy pixels. This occurs because during the restoration process the opening and closing by reconstruction smooth the pixels.

2. When only noise pixels are modified iteratively, the two algorithms (using the median and the ROM filter) take more time to execute. However, it is noteworthy to mention that the detection is carried out without considering fast algorithms.

3. The ROM filter applied iteratively on noisy pixels works better when the noise percentage is increased.

4. The output images produced with our proposal contain artifacts due to the performance of the median filter. An example of this can be observed in Fig. 4 where the contours were modified.

4 Conclusions and Future Work

In the Mathematical Morphology area, the noise elimination topic has not been dealt with in deep. Few transformations have been proposed in this theme. Therefore, an important contribution of this paper is the introduction of a methodology to restore images contaminated with impulse noise using morphological transformations. The proposal works iteratively and permits to obtain restored images where the structures of the image are better preserved if the noise percentage is low (10%). The structure preservation is due to i) treatment of only noisy pixels in each iteration, and ii) restoration of noisy pixels using extensive and antiextensive transformations. However, when the noise percentage is increased to 40 %, the ROM filter applied iteratively on noisy pixels produces

better results. This occurs since the output images obtained with our proposal are smoother due to the reconstruction transformations.

The disadvantage of detecting noise iteratively is that the algorithm consumes more time during its execution. The PSNR indices computed with our algorithm cannot increase more because the median filter used to filter the noisy images does not have the capability of adapting to the edges of the processed image placing as consequence a copy of several gray intensity levels around the contours. Also, our proposal does not have the capability of processing components smaller than the structuring element.

As future work, a fast algorithm and the proposal of an adaptative transformation to suppress noise will be taken into consideration.

Acknowledgements

The authors wish to thank the Mario Moreno Reyes foundation for the financial support. Iván R. Terol-Villalobos would like to thank Diego Rodrigo and Darío T.G. for their great encouragement. This work was funded by the government agency CONACyT (133697), México.

References

1. **Abreu, E., Lightstone, M., Mitra, S., & Arakawa, K.** (**1996**). A new efficient approach for the removal of impulse noise from highly corrupted images. *Image Processing, IEEE Transactions on*, Vol. 5, No. 6, pp. 1012–1025.
2. **Astola, J. & Kousmanen, P.** (**1997**). *Fundamentals of Nonlinear Digital Filtering*. Boca Raton, CRC.
3. **Chan, R., Ho, C.-W., Leung, C.-Y., & Nikolova, M.** (**2005**). Minimization of detail-preserving regularization functional by newton's method with continuation. *Image Processing, 2005. ICIP 2005. IEEE International Conference on*, volume 1, pp. I–125–8.
4. **Chen, T. & Wu, H. R.** (**2001**). Space variant median filters for the restoration of impulse noise corrupted images. *Circuits and Systems II: Analog and Digital Signal Processing, IEEE Transactions on*, Vol. 48, No. 8, pp. 784–789.
5. **Emre Celebi, M.** (**2009**). Real-time implementation of order-statistics-based directional filters. *Image Processing, IET*, Vol. 3, No. 1, pp. 1–9.
6. **Heijmans, H. J. A. M.** (**1994**). *Morphological image operators*. Advances in electronics and electron physics, supplement. Academic Press, Boston, MA.
7. **Hwang, H. & Haddad, R.** (**1995**). Adaptive median filters: new algorithms and results. *Image Processing, IEEE Transactions on*, Vol. 4, No. 4, pp. 499–502.
8. **Lerallut, R., Decencière, E., & Meyer, F.** (**2007**). Image filtering using morphological amoebas. *Image and Vision Computing*, Vol. 25, No. 4, pp. 395 – 404.
9. **Mendiola-Santibañez, J. D. & Terol-Villalobos, I. R.** (**2014**). Filtering of mixed gaussian and impulsive noise using morphological contrast detectors. *IET Image Processing*, Vol. 8, pp. 131–141.
10. **Mendiola-Santibañez, J. D., Terol-Villalobos, I. R., Jiménez-Sánchez, A. R., Gallegos-Duarte, M., Rodríguez-Reséndiz, J., & Santillán, I.** (**2011**). Application of morphological connected openings and levelings on magnetic resonance images of the brain. *International Journal of Imaging Systems and Technology*, Vol. 21, No. 4, pp. 336–348.
11. **Nikolova, M.** (**2004**). A variational approach to remove outliers and impulse noise. *Journal of Mathematical Imaging and Vision*, Vol. 20, No. 1-2, pp. 99–120.
12. **Sasaki, H.** (**2009**). A new flat pattern oriented order statistic filter for impulse noise reduction from highly corrupted images. *Proceedings of the IAPR Conference on Machine Vision Applications (IAPR MVA 2009), Keio University, Yokohama, Japan, May 20-22, 2009*, pp. 358–361.
13. **Serra, J.** (**2012**). Tutorial on connective morphology. *Selected Topics in Signal Processing, IEEE Journal of*, Vol. 6, No. 7, pp. 739–752.
14. **Shannon, C. E.** (**2001**). A mathematical theory of communication. *SIGMOBILE Mob. Comput. Commun. Rev.*, Vol. 5, No. 1, pp. 3–55.
15. **Terol-Villalobos, I. R.** (**2004**). Morphological connected contrast mappings based on top-hat criteria: a multiscale contrast approach. *Optical Engineering*, Vol. 43, No. 7, pp. 1577–1595.
16. **Vincent, L.** (**1993**). Morphological grayscale reconstruction in image analysis: applications and efficient algorithms. *Image Processing, IEEE Transactions on*, Vol. 2, No. 2, pp. 176–201.

17. **Vincent, L.** (**1994**). Morphological area openings and closings for grey-scale images. In **O, Y.-L., Toet, A., Foster, D., Heijmans, H., & Meer, P.**, editors, *Shape in Picture*, volume 126 of *NATO ASI Series*. Springer Berlin Heidelberg, pp. 197–208.
18. **Wang, Z., Bovik, A., Sheikh, H., & Simoncelli, E.** (**2004**). Image quality assessment: from error visibility to structural similarity. *Image Processing, IEEE Transactions on*, Vol. 13, No. 4, pp. 600–612.

Jorge Domingo Mendiola-Santibañez received the B.Sc. degree in Electronic Engineering from the Benemérita Universidad Autónoma de Puebla, México, his M.Sc. degree in Electronics from INAOE (México). He received his Ph.D. from the Universidad Autónoma de Querétaro (México). He is currently a researcher of Universidad Autónoma de Querétaro (Querétaro, México). His research interests include morphological image processing and computer vision.

Israel Marcos Santillán-Méndez received the B.S. degree in Engineering from the Instituto Tecnológico de Estudios Superiores de Monterrey, the M.S. degree in Engineering and Ph D in Engineering from Facultad de Ingeniería de la Universidad Autónoma de Querétaro (México). His research interests include models of biological sensory and perceptual systems and mathematical morphology.

Juvenal Rodríguez-Reséndiz received his MS degree in automation control from University of Querétaro and PhD degree at the same institution. Since 2004, he has been part of the Mechatronics Department at the UAQ. He is the head of the Automation Department. His research interest includes signal processing and motion control. He serves as vice president of IEEE in Queretaro State.

Miguel Octavio Arias-Estrada is a researcher in computer science at National Institute of Astrophysics, Optics and Electronics, Puebla, Mexico, with a PhD degree in electrical engineering (computer vision) from Laval University (Canada) and BEng and MEng degrees in electronic engineering from University of Guanajuato (Mexico). Currently, he is a researcher at INAOE (Puebla, México). His interests are computer vision, FPGA and GPU algorithm acceleration for threedimensional machine vision.

Martín Gallegos-Duarte is an MD and a PhD student at the Universidad Autonoma de Querétaro. He is head of the Strabismus Service at the Institute for the Attention of Congenital Diseases and Ophthalmology-Pediatric Service in the Mexican Institute of Ophthalmology in the state of Queretaro, Mexico.

Domingo José Gómez-Meléndez received his PhD degree from the Universidad Autónoma de Querétaro (UAQ), México. Currently, he is a professor/researcher at the Universidad Autónoma de Querétaro. His research interests include image processing and greenhouses.

Iván Ramón Terol-Villalobos received his B.Sc. degree from Instituto Politécnico Nacional (I.P.N. México), his M.Sc. degree in Electrical Engineering from Centro de Investigación y Estudios Avanzados del I.P.N. (México), and a DEA in Computer Science from the University of Paris VI (France). He received his Ph.D. degree from the Centre de Morphologie Mathématique, Ecole des Mines de Paris (France). He is currently a researcher of Centro de Investigación y Desarrollo Tecnológico en Electroquímica (Querétaro, México). His main current research interests include morphological image processing, morphological probabilistic models, and computer vision.

Article received on 22/11/2013; accepted on 09/03/2015.
Corresponding author is Jorge Domingo Mendiola-Santibañez.